Journal of Engineering Mathematics **40:** 283–296, 2001.

Towards approximate models of Coulomb frictional moments in: (I) revolute pin joints and (II) spherical-socket ball joints

ALI FARAZ and SHAHRAM PAYANDEH
Experimental Robotics Laboratory (ERL), School of Engineering Science, Simon Fraser University, 8888 University Drive, Burnaby, British Columbia, Canada V5A 1S6 (e-mail: shahram@cs.sfu.ca)

Received 15 April 1999; accepted in revised form 1 October 2000

Abstract. In general, the rigid-contact assumption has been used to estimate the frictional moment between two bodies in contact. In a multi-body connection, two types of passive interconnection are considered in this paper, namely pin joint and spherical-ball joint. The joints are assumed to be passive at the localized configuration space of the multi-body systems and are assumed to be actuated remotely. The traditional approach for modelling such frictional contact does not consider the elastic deformation of joints. Two approximate models are presented for both revolute pin joints and spherical-socket ball joints. The proposed models offer a more accurate estimation of the Coulomb frictional moment. The new models offer a compact solution which can be easily extended to other geometrical multi-body contact configurations with various degrees of clearance. The proposed models can be used in the dynamic modelling and control of multi-body systems in frictional contact.

Key words: approximate frictional models, pin joints, spherical joints

1. Introduction

In general, all linkaged mechanisms and multi-body systems consist of joints and linkages. Rotary joints are the most commonly used type of joints. Rotary joints consist of two general categories: (a) revolute joints (providing one Degree of Freedom (DOF)), and (b) spherical joints (providing up to three DOF). Specifically, the revolute pin joints and spherical socket-ball joints are used when the requirements include: (a) relatively high radial loads at the joints, (b) very high stiffness of the joints to reduce the vibrational tendencies of the system, and (c) simple and compact joints design. However, these two types of joints have disadvantages (when compared to low-friction bearings with intermediate rolling elements) such as: (a) lower operational speed, (b) relatively shorter service life, and (c) higher friction. For modelling and analysis of such joints, it is required to estimate/predict the frictional moment in these joints. The motivation for the need to accuratly model the frictional moments can be further explained using the following examples:

(I) In the static cases (*e.g.* truss-cell systems [1], or endoscopic multi-jointed devices [2–3]), it is desired to predict/estimate the maximum frictional moment capacity of the locked joints under different loading conditions.

(II) In the dynamic cases of multi-body systems, the frictional moment at each joint is a contributing factor in the dynamic model between bodies. For accurate modeling of the system, it is essential to model frictional moment with the required accuracy [4–6].

(III) Another specific example (with both static and dynamic applications) is the flexible stem in endoscopic tools which consist of several spherical joints (Figure 1). This design allows the tools tip to have two degrees of freedom. Each joint is actuated by tendon-like

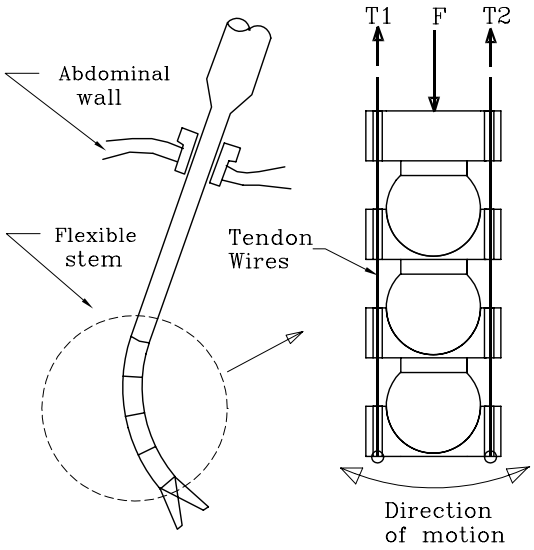

Figure 1. The flexible stem of an endoscopic tool.

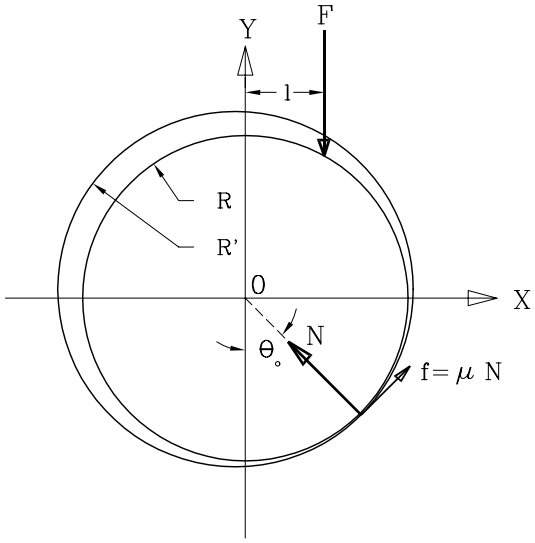

Figure 2. The rigid joint under load F.

wires at the periphery. The unique feature of this design is that these joints are held together, moved, and locked by changing the tension in the tendons. In the static case, when the joints are locked, the tension in the wires should exceed some minimum limit in order to prevent the joints from any slipping. However, in the dynamic case of moving joints, the tension must be reduced in some of the wires to allow the joints to rotate in the desired direction. In both of these cases it is important to estimate accurately the frictional moments of joints which are controlled by the tension of tendons.

As mentioned above, there are several papers related to experimental applications/studies of Coulomb frictional moment of joints [2], [6], [1], as well as general theoretical studies [4–5]. Reference [12, Section 4.1, Chapter 7] is a good reference book on general modelling and solution of various contact-mechanics problems. In all of these works, it is assumed that joints are absolutely rigid, and the contact is modeled as a point contact in the spherical socket-ball joints, and a line contact in revolute ones, where all the frictional force is concentrated on. This has led to simplified models for predicting the frictional moment. Various approaches have been also followed to model approximately the Coulomb and stress model for Hertzian contact with compliant model approximation. For example, Lukowski *et al.* [7] analyzes the contact stresses and contact area of mating disks in frictional transmission. Approximate Hertz formulations are adopted to determine the maximum contact stresses under elastic deformation. Another approach for such approximations is given in [8]. Here a simple method is presented for analysis of contact stresses and deformation between the bearing balls, screw and nut of the screw mechanism. Simplified Hertzian contact solutions are obtained using curvature information. Similar approximations to the contact model between elastic bodies can be found in [9–11].

However, in general there is a contact area caused by the elastic deformation of the joint that the Coulomb friction is acted on instead of the point contact. In this paper, contacts in the joints are considered elastic and by use of the elliptic load distribution over the contact surfaces, approximate models are developed which can predict/estimate the frictional moments

with better accuracy. Finally, mathematical models for estimating the range of clearance in the joints that ensures full contact and maximum stiffness of the pin and socket-ball joints are presented.

2. Preliminary analysis

A simple derivation of the current model is demonstrated here by the assumption of absolute rigidity of the joint with a point contact between its surfaces (Figure 2, gives a cross-sectional view for both cases). The force F is the resultant external load acting on the joint (Figure 2), and the basic equilibrium of forces and moments for both cases are:

$$\sum F_x = -N \sin\theta_0 + \mu N \cos\theta_0 = 0,$$
$$\sum F_y = N \cos\theta_0 + \mu N \sin\theta_0 = F,$$
$$\sum M_o = \mu N R = Fl,$$

where $N =$ the reaction force at the contact point, $l =$ the distance of force F to the center of joint, $\theta_0 =$ the equilibrium angle of contact point, $\mu =$ the coefficient of friction between the two surfaces of joint.

The first equation leads to: $\tan\theta_0 = \mu$, and solving the other two equations provides: $N = F/\sqrt{1+\mu^2}$, and:

$$\frac{l}{R} = \frac{\mu}{\sqrt{1+\mu^2}}. \tag{1}$$

Using the above equations, we can obtain the frictional moment acting on the joint ($M = \mu N R$) as:

$$M = F \times R \frac{\mu}{\sqrt{1+\mu^2}}, \tag{2}$$

and for small values of μ (*e.g.*, $\mu < 0{\cdot}3$), the value of $\sqrt{1+\mu^2}$ can be approximated to be equal to 1; Equations (1) and (2) reduce to: $l/R = \mu$, and $M = \mu F R$.

Equation (2) is used extensively in the literature ([1–2], [4–6]) to predict the frictional moment in revolute or spherical joints. However, the above simplified analysis does not consider the elasticity of the joints. The following sections take into account the effects of elastic deformation and stress distribution over the contact area in revolute pin joints, and spherical socket-ball joints, in order to estimate the Coulomb frictional moment more realistically, and with higher accuracy.

3. Revolute pin joints

This section first presents the study of the stress distribution on the contact area of revolute joint; then, by applying the Coulomb friction law at the contact area, the equilibrium analysis is carried out.

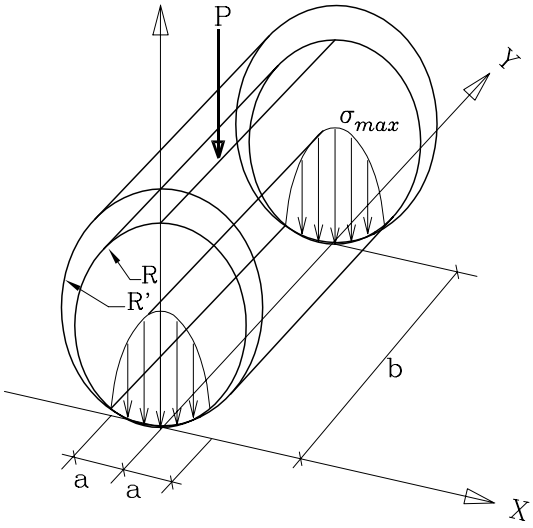

Figure 3. The stress distribution between two cylindrical surfaces.

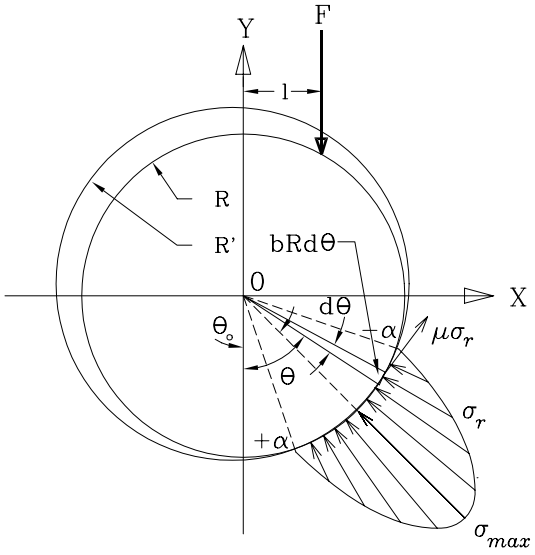

Figure 4. The revolute pin joint under load F.

3.1. THE RADIAL STRESS DISTRIBUTION

The radial contact stress σ_r between the two cylindrical surfaces of radiuses R and R' due to deformation are known [13, pp. 151–160], [15, pp. 81–88] to have an elliptical distribution expressed as follows:

$$\sigma_r = \sigma_{\max}\sqrt{1 - \frac{x^2}{a^2}}. \tag{3}$$

When the materials of the two surfaces are the same, with the elastic modulus E and Poisson ratio $\nu \approx 0{\cdot}3$ (true for most alloys), the maximum radial stress $\sigma_{\max}$ at the center line the of contact region is:

$$\sigma_{\max} = 0{\cdot}418\left[\frac{PE}{b}\left(\frac{R' - R}{RR'}\right)\right]^{1/2}, \tag{4}$$

and the width of the contact area ($= 2a$, Figure 3) can be obtained by:

$$a = R\sin\alpha = 1{\cdot}25[\frac{P}{Eb}\frac{R'R}{R' - R}]^{1/2}, \tag{5}$$

where: b = The axial width of the revolute joint (Figure 3), $P = F\cos\theta_0$ = The radial component of load F, α = Half of the maximum angular contact between the two cylinders (Figure 4).

With different elastic moduli of E_1, E_2 and Poisson ratios ν_1, ν_2, then E in the above equation is replaced by $1{\cdot}82E_1E_2/((1 - \nu_2^2)E_1 + (1 - \nu_1^2)E_2)$, [15].

We used Equation (3) for obtaining the radial stress distribution. It is assumed that the Coulomb frictional law can be used for obtaining the tangential stress distribution between two cylindrical surfaces of the joint.

3.2. EQUILIBRIUM ANALYSIS

Given the stress distributions on cylindrical surfaces, it is possible to write down equilibrium equations of forces and moments. The components of forces acting on an infinitesimal area of contact $bR\mathrm{d}\theta$ (Figure 4) are:

$$\sum \vec{\mathbf{dF}} = \sigma_r bR\,\mathrm{d}\theta[(\mu\cos\theta - \sin\theta)\hat{\mathbf{i}} + (\cos\theta + \mu\sin\theta)\hat{\mathbf{j}}], \tag{6}$$

where $\sigma_r = \sigma_{\max}\sqrt{1 - \frac{R^2}{a^2}\sin^2(\theta - \theta_0)}$ is obtained from Equation (3).

By integration over the contact area, equilibrium equations of forces along X, Y, and moment around Z axis (Figure 4) can be written as:

$$\begin{aligned}\sum \mathbf{F}_x &= \int_{\theta_0-\alpha}^{\theta_0+\alpha} \sum \vec{\mathbf{dF}} \cdot \hat{\mathbf{i}} \\ &= \int_{\theta_0-\alpha}^{\theta_0+\alpha} bR\sigma_{\max}(\mu\cos\theta - \sin\theta)\sqrt{1 - \frac{R^2}{a^2}\sin^2(\theta - \theta_0)}\,\mathrm{d}\theta = 0,\end{aligned} \tag{7}$$

$$\begin{aligned}\sum \mathbf{F}_y &= \int_{\theta_0-\alpha}^{\theta_0+\alpha} \sum \vec{\mathbf{dF}} \cdot \hat{\mathbf{j}} \\ &= \int_{\theta_0-\alpha}^{\theta_0+\alpha} bR\sigma_{\max}(\mu\sin\theta + \cos\theta)\sqrt{1 - \frac{R^2}{a^2}\sin^2(\theta - \theta_0)}\,\mathrm{d}\theta = F,\end{aligned} \tag{8}$$

$$\begin{aligned}\sum \mathbf{M}_o &= \int_{\theta_0-\alpha}^{\theta_0+\alpha} \left[\vec{\mathbf{R}} \times \sum \vec{\mathbf{dF}}\right] \cdot \hat{\mathbf{k}} \\ &= \int_{\theta_0-\alpha}^{\theta_0+\alpha} \mu bR^2\sigma_{\max}\sqrt{1 - \frac{R^2}{a^2}\sin^2(\theta - \theta_0)}\,\mathrm{d}\theta = Fl,\end{aligned} \tag{9}$$

where: $\theta_0 =$ the angle where maximum radial stress occurs (Figure 4). $\vec{\mathbf{R}} = R(\sin\theta\hat{\mathbf{i}} - \cos\theta\hat{\mathbf{j}})$, $l =$ the distance between force F and y axis (Figure 4).

By setting $a = R\sin\alpha$ and $u = \theta - \theta_0$, Equations (7) and (8) can be solved and we have:

$$\tan\theta_0 = \mu, \tag{10}$$

$$F = \frac{\pi bR}{2}\sigma_{\max}(1 + \mu^2)^{1/2}\sin\alpha. \tag{11}$$

On the other hand, Equation (9) can not be solved analytically, since it is an elliptic integral. There are various approaches of finding the solution for (9).

I) Numerical integration: This method could be applied by means of numerical integration algorithms to each individual case; however, it is computationally expensive, and time-consuming. This is true when the solution is needed for dynamic cases (such as the endoscopic flexible extenders), where load and other parameters are constantly changing.

II) Tabulated values: There are tables for different kinds of elliptic integrals that could be used ([14, pp. 299–301]) to solve Equation (9). Although impractical, they are used in this paper (Table 1) to verify the results of the next method (*Expansion Series*) and, based on that, develop a convenient approximate solution.

III) Expansion series: Approximation is possible by obtaining a series expansion of Equation (9). For this purpose first let $K = R/a$ and $u = \theta - \theta_0$ render Equation (9) in the following form:

$$\frac{Fl}{\mu b R^2 \sigma_{\max}} = \int_{-\alpha}^{\alpha} \sqrt{1 - K^2 \sin u^2}\, \mathrm{d}u = 2\mathcal{E}(\alpha, K), \tag{12}$$

where $\mathcal{E}(\alpha, K)$ is defined as *the normal elliptic integral of the second kind* [14] that could be represented by an expansion series if $K < 1$. However, in our case $K \geq 1$ since: $K = R/a$, and $a = R \sin\alpha$, so $K = 1/\sin\alpha$, since $1 \geq \sin\alpha \geq 0$ which results in: $K \geq 1$. Therefore, it is necessary to use a *Reciprocal Modulus Transformation* [14] of $\mathcal{E}(\alpha, K)$ as $\mathcal{E}(\alpha, K) = [\mathcal{E}(\beta, k) - (1-k^2)\mathcal{F}(\beta, k)]/k$, where $k = 1/K = \sin\alpha$, and $\beta = \sin^{-1}(K \sin\alpha) = \sin^{-1}(1) = \pi/2$. Also $\mathcal{F}(\beta, k)$ is *the normal elliptic integral of the first kind*. Then Equation (12) is transformed to:

$$\frac{Fl}{\mu b R^2 \sigma_{\max}} = 2\mathcal{E}(\alpha, K) = 2[\mathcal{E}(\pi/2, k) - (1 - k^2)\mathcal{F}(\pi/2, k)]/k. \tag{13}$$

Now by substituting (11) in (13), we can further reduce the expansion as:

$$\frac{l}{R} = \frac{4\mathcal{E}(\alpha, K)}{\pi \sin\alpha} \frac{\mu}{\sqrt{1+\mu^2}} = C_\alpha \frac{\mu}{\sqrt{1+\mu^2}}, \tag{14}$$

where

$$C_\alpha = \frac{4\mathcal{E}(\alpha, K)}{\pi \sin\alpha} = \frac{4}{\pi}[\mathcal{E}(\pi/2, k) - (1 - k^2)\mathcal{F}(\pi/2, k)]/k^2. \tag{15}$$

We can use the expansion series of $\mathcal{E}$ and $\mathcal{F}$ [14] to obtain an expansion series for C_α by applying them to Equation (15) as follows:

$$\begin{aligned}
&\mathcal{E}(\pi/2, k) = \tfrac{\pi}{2}\left[1 - \tfrac{1}{4}k^2 - \tfrac{3}{64}k^4 - \tfrac{5}{256}k^6 - \tfrac{175}{16384}k^8 - \cdots\right],\\
&\mathcal{F}(\pi/2, k) = \tfrac{\pi}{2}\left[1 + \tfrac{1}{4}k^2 + \tfrac{9}{64}k^4 + \tfrac{25}{256}k^6 + \tfrac{1225}{16384}k^8 + \cdots\right],\\
&C_\alpha = 1 + \tfrac{1}{8}k^2 + \tfrac{3}{64}k^4 + \tfrac{25}{1024}k^6 + \tfrac{245}{16384}k^8 + \cdots.
\end{aligned} \tag{16}$$

On the other hand, the tabulated values of $\mathcal{E}$ and $\mathcal{F}$ [14] are used, and the following values of C_α based on Equation (15) are calculated (Table 1) and plotted *vs.* α in Figure 5 (shown by small circles).

Comparing the results of these two approaches shows that the series (16) converges to the final values of C_α (Table 1) very slowly as the number of elements in the series are increased. For example, even the summation of the first five elements of the series results in a 5% deviation for large values of α (as shown by the dashed line A in Figure 5) from the tabulated values.

IV) Curve fitting : By curve-fitting techniques (to the data points of C_α from Table 1) it is possible to obtain functions with better accuracy compared to the results of the expansion series with a limited number of elements. For example, by knowing the type of polynomial obtained from previous section (*i.e.*, Equation (16)), we could solve the function $C_\alpha = 1 + Ak^2 + Bk^4 + Ck^6 + Dk^8$ by a least-squares method for the tabulated values of C_α (from Table 1) to obtain the coefficients A, B, C, and D. This results in:

$$C_\alpha = 1 + 0{\cdot}0477k^2 + 0{\cdot}5744k^4 - 1{\cdot}051k^6 + 0{\cdot}6982k^8. \tag{17}$$

Table 1. The values of C_α for different contact angles α .

α	$k = \sin\alpha$	$\mathcal{E}(\pi/2, k)$	$\mathcal{F}(\pi/2, k)$	$2\mathcal{E}(\alpha, K)$	C_α
0	0·0	1·57080	1·570796	0·0000	1·000
5	0·087	1·567809	1·573792	0·1370	1·001
15	0·259	1·544150	1·598142	0·4100	1·008
30	0·500	1·467462	1·685750	0·8126	1·035
45	0·707	1·350644	1·854075	1·1981	1·079
60	0·866	1·211056	2·156516	1·5517	1·141
75	0·966	1·076405	2·768063	1·8448	1·216
90	1·000	1·00000	∞	2·0000	1·273

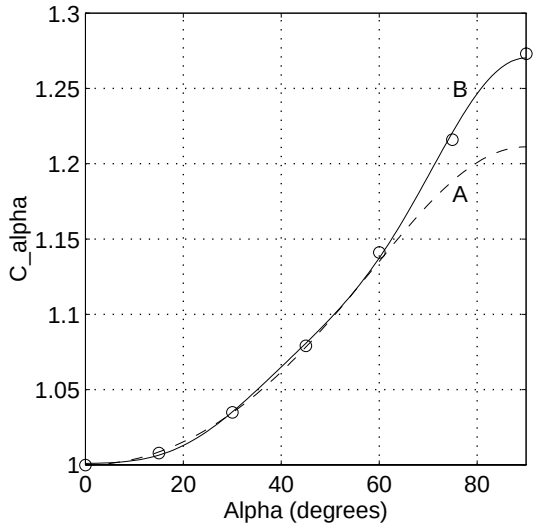

Figure 5. C_α *vs.* α for revolute pin joints.

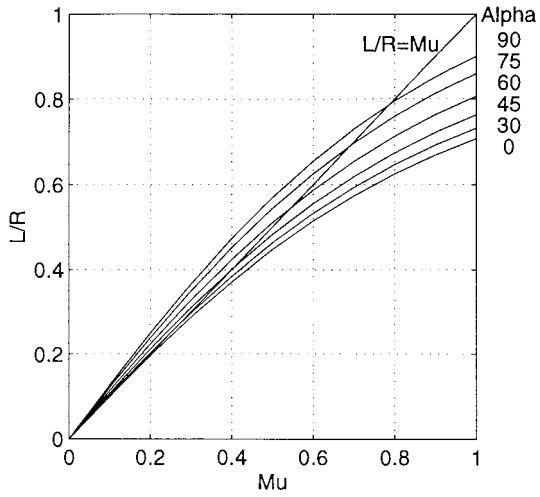

Figure 6. l/R *vs.* μ for revolute pin joints.

The above equation has less than 1% deviation from the values of C_α over the whole range of α (shown by the solid line B in Figure 5). This is a reasonable level of accuracy for most practical applications, but other optimal curve-fitting techniques might even achieve higher accuracies.

Now, by having the equation of C_α, we can write the final frictional moment of the revolute pin joint as:

$$\begin{aligned} M &= F \times l \\ &= F \times R(1 + 0{\cdot}0477\sin^2\alpha + 0{\cdot}5744\sin^4\alpha - 1{\cdot}051\sin^6\alpha + \\ &\quad + 0{\cdot}6982\sin^8\alpha)\frac{\mu}{\sqrt{1+\mu^2}}, \end{aligned} \tag{18}$$

where α can be obtained from (5) and (10) as:

$$\alpha = \sin^{-1}\left[\left(\frac{2{\cdot}31\mathrm{F}}{Eb\sqrt{1+\mu^2}}.\frac{R'/R}{R'-R}\right)^{1/2}\right].$$

From the above equation it is evident that the value of M for some specific force F depends only on the parameter l. So the ratio l/R ($= M/FR$) can be considered as a dimensionless index that represents the maximum moment capacity of the joint, regardless of the revolute-joints dimensions.

The quantity l/R from Equation (14) is plotted for different values of μ and α in Figure 6. In this plot the curve corresponding to $\alpha = 0$ represents the rigid-joint model, since, for $\alpha = 0$: $C_\alpha = 1$, and Equation (14) converts to Equation (1), and when it is compared to the full contact case (where $\alpha = 90°$), Equation (1) has a deviation of 21% from Equation (18). This could result in the same amount of error, if Equation (1) is used for a full-contact case. Actually, the straight-line approximation $l/R = \mu$ provides a much better approximation for near full-contact conditions than Equation (1). However, there is no need for approximation anymore, as the new model (18) provides an accurate estimate of M for any condition of friction and contact angle.

4. Spherical socket-ball joints

In this section, a similar procedure as that of Section 3 is applied to spherical socket-ball joints. First, the stress distribution on the contact area of a spherical joint is studied; then, through application of Coulomb's friction law at the contact area, the equilibrium analysis is carried out.

4.1. The radial stress distribution

Similar to the cylindrical case (Equation (3)), the radial contact stress σ_r between the two spherical surfaces of radii R and R' due to deformation are known ([13], [15]) to be an elliptical distribution as well. However, the elliptic distribution is along two axes (*i.e.*, X and Y axis) :

$$\sigma_r = \sigma_{\max}\sqrt{1-\frac{x^2}{a^2}-\frac{y^2}{a^2}}. \tag{19}$$

When the materials of the two surfaces are the same, with the elastic modulus E and Poisson ratio $\nu \approx 0{\cdot}3$ (true for most alloys), the maximum radial stress $\sigma_{\max}$ at the center of the contact region is:

$$\sigma_{\max} = 0{\cdot}389\left[PE^2\left(\frac{R-R'}{RR'}\right)^2\right]^{1/3}, \tag{20}$$

and the radius of the contact region ($= a$, Figure 7) can be obtained from:

$$a = R\sin\alpha = 1{\cdot}11\left[\frac{P}{E}\frac{RR'}{R-R'}\right]^{1/3}, \tag{21}$$

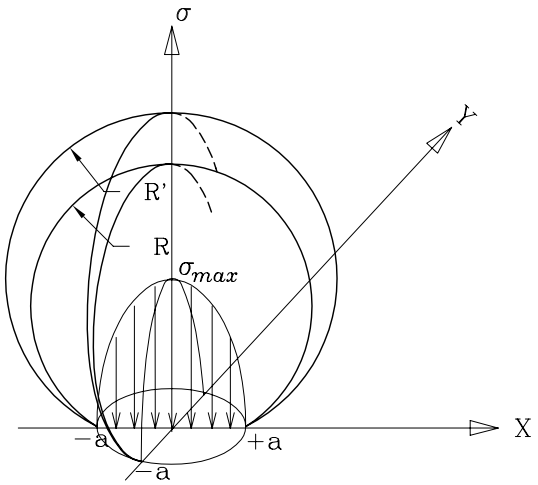

Figure 7. The stress distribution between two spherical surfaces.

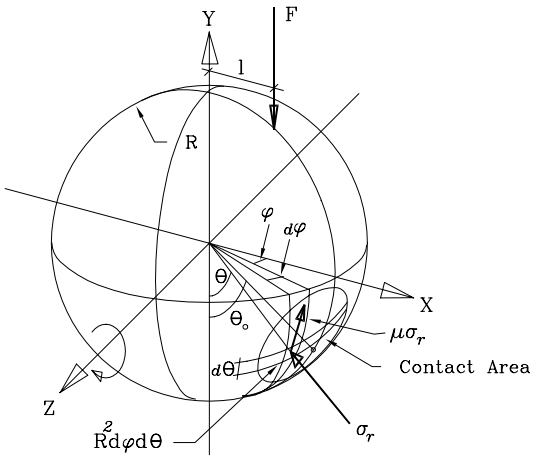

Figure 8. The spherical socket ball joint under load F.

where: $P = F cos\theta_0 =$ the radial component of F. $\alpha =$ half of the maximum contact angle between the two spheres.

However, if the materials of the two surfaces are not the same, then E in the above equation has to be changed into $1{\cdot}82E_1E_2/((1-\nu_2^2)E_1 + (1-\nu_1^2)E_2)$ as described in Section 3.1.

4.2. Equilibrium analysis

Based on the stress distribution on the spherical surface, we can obtain the equilibrium equations of forces and moments, first, by considering forces acting on an infinitesimal area, then integrating it over the whole contact area. The components of the forces (normal and frictional tangent forces) acting on an infinitesimal area of contact $R^2 \mathrm{d}\phi\ \mathrm{d}\theta$ (Figure 8) are:

$$\sum \vec{\mathbf{dF}} = \sigma_r R^2 \left[(-\cos\phi \sin\theta \hat{\mathbf{i}} + \cos\theta \cos\phi \hat{\mathbf{j}} - \sin\phi \hat{\mathbf{k}}) + \mu(\sin\theta \hat{\mathbf{j}} + \cos\theta \hat{\mathbf{i}}) \right] \mathrm{d}\phi\, \mathrm{d}\theta. \quad (22)$$

By integrating over the contact area, we may write the equilibrium equations of forces along x, y, and moment around z-axis (Figure 6) as:

$$\begin{aligned} \sum \vec{\mathbf{F}}_x &= \int_{\theta_0-\alpha}^{\theta_0+\alpha} \int_{-\alpha'}^{+\alpha'} \sum \vec{\mathbf{dF}} \cdot \hat{\mathbf{i}} \\ &= \int_{\theta_0-\alpha}^{\theta_0+\alpha} \int_{-\alpha'}^{+\alpha'} R^2 \sigma_r (\mu \cos\theta - \cos\phi \sin\theta)\, \mathrm{d}\phi\, \mathrm{d}\theta = 0, \end{aligned} \quad (23)$$

$$\begin{aligned} \sum \vec{\mathbf{F}}_y &= \int_{\theta_0-\alpha}^{\theta_0+\alpha} \int_{-\alpha'}^{+\alpha'} \sum \vec{\mathbf{dF}} \cdot \hat{\mathbf{j}} \\ &= \int_{\theta_0-\alpha}^{\theta_0+\alpha} \int_{-\alpha'}^{+\alpha'} R^2 \sigma_r (\cos\theta \cos\phi + \mu \sin\theta)\, \mathrm{d}\phi\, \mathrm{d}\theta = F, \end{aligned} \quad (24)$$

$$\sum \vec{\mathbf{M}}_{\mathbf{z}} = \int_{\theta_0-\alpha}^{\theta_0+\alpha} \int_{-\alpha'}^{+\alpha'} \left[\vec{\mathbf{R}} \times \sum \vec{\mathbf{dF}}\right] \cdot \hat{\mathbf{k}} = \int_{\theta_0-\alpha}^{\theta_0+\alpha} \int_{-\alpha'}^{+\alpha'} \mu R^2 \sigma_r \cos\phi \, \mathrm{d}\phi \, \mathrm{d}\theta = Fl, \qquad (25)$$

where, $\sigma_r = \sigma_{\max}\sqrt{1-[\frac{R}{a}\sin(\theta-\theta_0)]^2-[\frac{R}{a}\sin\phi]^2}$, $\vec{\mathbf{R}} = R(\cos\phi\sin\theta\hat{\mathbf{i}} - \cos\phi\cos\theta\hat{\mathbf{j}} + \sin\phi\hat{\mathbf{k}})$, $l =$ the distance between force F and y axis (Figure 8), $\theta_0 =$ the angular position of center of the contact area(Figure 8), $\alpha' = \sin^{-1}\sqrt{\sin^2\alpha - \sin^2(\theta-\theta_0)}$.

After expansion of the Equations (23) and (24), they are converted into elliptic integral forms which do not have analytical solutions. However, it is possible to verify numerically that Equation (23) leads to the same equation: $\tan\theta_0 = \mu$, for different values of μ and α. Now, by knowing $\theta_0 = \tan^{-1}\mu$, it is possible to find the radial component of force F (*i.e.*, $P = F\cos\theta_0$), which drives the two spherical surfaces into each other radially, and is the same as force P in Equations (20) and (21). As a result we can have:

$$P = F\cos\theta_0 = F/\sqrt{1+\mu^2}.$$

On the other hand, by multiplying Equation (20) by the square of Equation (21), we may obtain a relation between $\sigma_{\max}$ and P as:

$$\sigma_{\max}(R\sin\alpha)^2 = 0{\cdot}388(1{\cdot}11)^2\left[P^3(\frac{E\Delta RR}{ER\Delta R})^2\right]^{1/3} = 0388(1{\cdot}11)^2P.$$

Replacing $P = F/\sqrt{1+\mu^2}$ in the above equation, a relationship between F, and $\sigma_{\max}$ can be obtained without solving Equation (24) as follows:

$$\sigma_{\max} = \frac{0{\cdot}388(1{\cdot}11)^2}{R^2\sin^2\alpha\sqrt{1+\mu^2}}F. \qquad (26)$$

Now by substituting $\sigma_{\max}$ given by (26) in the trigonometric form of Equation (19), we can write

$$\begin{aligned}\sigma_r &= \sigma_{\max}\sqrt{1-\left[\frac{R}{a}\sin(\theta-\theta_0)\right]^2-\left[\frac{R}{a}\sin\phi\right]^2} \\ &= \frac{0{\cdot}388(1{\cdot}11)^2}{R^2\sin^2\alpha\sqrt{1+\mu^2}}F\sqrt{1-\left[\frac{R}{a}\sin(\theta-\theta_0)\right]^2-\left[\frac{R}{a}\sin\phi\right]^2},\end{aligned}$$

which provides us with σ_r, which can be used in Equation (25). This makes it possible to integrate Equation (25), and obtain:

$$\pi\mu\frac{0{\cdot}388(1{\cdot}11)^2}{R^2\sin^2\alpha\sqrt{1+\mu^2}}FR^3\left[\cos\alpha - \alpha\frac{\cos 2\alpha}{\sin\alpha}\right] = Fl.$$

After simplification it leads to:

$$\frac{l}{R} = 0{\cdot}75\left[\frac{\cos\alpha}{\sin^2\alpha} - \alpha\frac{\cos 2\alpha}{\sin^3\alpha}\right]\frac{\mu}{\sqrt{1+\mu^2}}. \qquad (27)$$

Equation (27) has the same basic structure as Equation (14) in the case of revolute pin joint (*i.e.*, $l/R = C_\alpha\mu/\sqrt{1+\mu^2}$). However, in this case C_α is

$$C_\alpha = 0{\cdot}75\left[\frac{\cos\alpha}{\sin^2\alpha} - \alpha\frac{\cos 2\alpha}{\sin^3\alpha}\right]. \qquad (28)$$

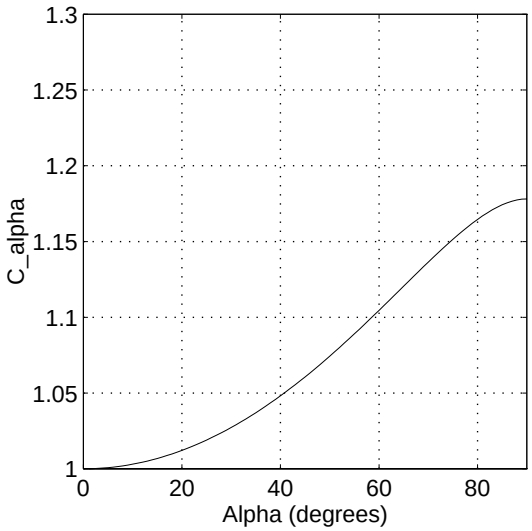

Figure 9. C_α *vs.* α for spherical-socket ball joints.

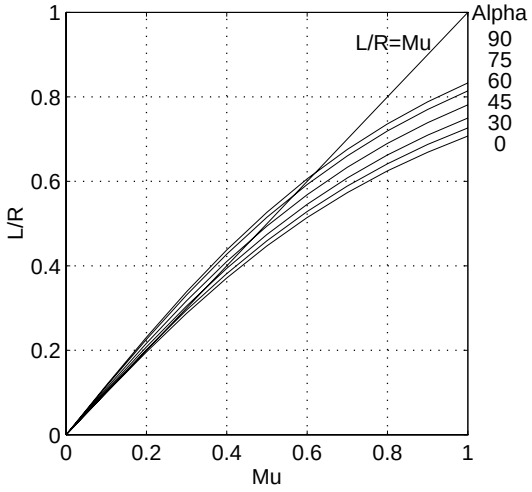

Figure 10. l/R *vs.* μ for spherical-socket ball joints.

C_α is plotted *vs.* α in Figure 9, which can be interpreted as the deviation of the elastic joint (as a more realistic assumption) from the absolute rigid joint (as an ideal-case assumption, where $C_\alpha = 1$).

Now, by use of Equation (28), the frictional moment of the spherical joint would be:

$$M = F \times l = \frac{3}{4} F \times R \left[\frac{\cos\alpha}{\sin^2\alpha} - \alpha \frac{\cos 2\alpha}{\sin^3\alpha} \right] \frac{\mu}{\sqrt{1+\mu^2}}, \tag{29}$$

where, α can be obtained from (21) as

$$\alpha = \sin^{-1} \left[\left(\frac{1{\cdot}367F}{ER\Delta R\sqrt{1+\mu^2}} \right)^{1/3} \right].$$

Similar to the previous section, l/R is the dimensionless parameter that represents the frictional moment capacity, M, of the spherical-socket ball joint regardless of its size. Hence, l/R of Equation (27) is plotted for different values of μ and α as shown in Figure 10. In this plot, the curve corresponding to $\alpha = 0$, represents the rigid-joint model, and, as compared to full contact case (where $\alpha = 90°$), Equation (1) has a deviation of about 15%. This means that Equation (1) will result in a 15% error, if used when the joint is in full contact.

5. Discussions

Based on the previous analysis, we have presented mathematical models (Equations (18), and (29)) that can predict the frictional moment M of the joints as a function of the contact angle α, and μ. However, to apply these models effectively, it is important to know under what range

of loads on the joint, the value of α(and subsequently C_α, and M) is affected most. To clarify this in more detail the following questions must be addressed and discussed:

I) In what minimal range of loads does the joint still behaves as a rigid joint (*i.e.*, $\alpha \approx 0$ and $C_\alpha \approx 1$)?

II) In what intermediate range of loads does the joint have partial contact as an elastic joint (*i.e.*, $0 < \alpha < 90°$)?

III) In what maximal range of loads does the joint have full contact as an elastic joint (*i.e.*, $\alpha = 90°$)?

In order to answer the above questions, first, we have to find the maximum load capacity of the joint $P_{\max}$, as an upper bound limit, as well as a relative scale of comparison for other smaller loads(as the ratio $P/P_{\max}$). The reason that P has been used here instead of the load force F is that the radial load $P(= F\cos\theta_0)$ is the only contributing component of load F which is used in the computation of $\sigma_{\max}$ in Equations (4) and (20).

Let us first consider the revolute pin joints. Based on the strength of material(as the design criteria for maximum loading of joints), the maximum radial force $P_{\max}$ that can be exerted on the joint must not induce larger stresses than the allowable stress σ_y/S, where σ_y is the yield stress of the joint's material and S is the safety factor of design. Therefore $\sigma_{\max}$ in Equation (4) can be replaced by σ_y/S in order to find the maximum value of P defined as $P_{\max}$. As a result we have:

$$P_{\max} = \frac{5{\cdot}72b(R\sigma_y)^2}{E\Delta RS^2}. \tag{30}$$

Here $\Delta R = R' - R$, and $R' \simeq R$ is assumed.

On the other hand, the full contact between the two cylindrical surfaces of the joint happens when the contact angle is 180° (*i.e.*, $\alpha = 90°$, Figure 4). Here, P_{fc} is defined as the minimum radial force required to cause *full contact* in the joint (*i.e.*, $\alpha = 90°$). We can obtain a relation for P_{fc} by substituting $\alpha = 90°$ in Equation (5), namely $a = R\sin(90°) = 1{\cdot}52[\frac{P_{fc}}{Eb}\frac{RR'}{\Delta R}]^{1/2}$ and by assuming $R' \simeq R$, we have for P_{fc}:

$$P_{fc} \geq \frac{Eb\Delta R}{2{\cdot}31}. \tag{31}$$

Now by dividing (31) by (30) and for revolute pin joints we can obtain the ratio of P_{fc} and $P_{\max}$ as:

$$1 \geq \frac{P_{fc}}{P_{\max}} \geq 0{\cdot}076\left[S\frac{\Delta R}{R}\frac{E}{\sigma_y}\right]^2. \tag{32}$$

The same can be done for spherical socket-ball joints yielding the following:

$$1 \geq \frac{P_{fc}}{P_{\max}} \geq 0{\cdot}043\left[S\frac{\Delta R}{R}\frac{E}{\sigma_y}\right]^3. \tag{33}$$

As an example, let us look at a steel joint with normal design parameters such as: $\sigma_y = 500$ MPa, $E = 210$ GPa, $R = 10$ mm, $\Delta R = 0{\cdot}01$ mm, and the design safety factor of $S = 2{\cdot}5$. Table 2 shows typical calculated values for α, C_α, and $P/P_{\max}$ for the revolute and

Table 2. The typical calculated values of C_α, α, and $P/P_{\max}$.

Type	Revolute Pin Joint			Spherical Socket-Ball Joint		
Contact	Low	Partial	Full	Low	Partial	Full
C_α	1·0 – 1·01	1·01 – 1·27	$1{\cdot}273 = \frac{4}{\pi}$	1·0 – 1·01	1·01 – 1·17	$1{\cdot}178 = \frac{3\pi}{8}$
α	0 – 20	21 – 89	90	0 – 18	19 – 89	90
$\frac{P}{P_{\max}}$	0 – 0·01	0·01 – 0·08	0·08 – 1·0	0 – 0·001	0·001 – 0·05	0·05 – 1·0

spherical cases. In this table, low contact refers to the narrow range of α that corresponds to the range of $1 \leq C_\alpha \leq 1{\cdot}01$. In other words, the low contact range represents the range of α (and the corresponding values of $P/P_{\max}$) in which $C_\alpha \simeq 1$, and the joint is still behaving rigid under the very light load. The partial contact is defined as the range for which the contact angle α is more than that for the low contact range, but less than full contact(that $\alpha = 90^\circ$).

For revolute pin joints, it is apparent from the above example that, for the assumption of rigid joint to be accurate ($C_\alpha \simeq 1$), P should not exceed 1% (and 0·1%, in the case of spherical joints) of the maximum allowable load $P_{\max}$.

On the other hand, in the full contact columns, when the load P exceeds 8% and 5% of $P_{\max}$, C_α is equal to 1·273, and 1·178 for revolute and spherical joints, respectively. This is more than 90% of the range of allowable load $P_{\max}$. Therefore, assuming $C_\alpha = 1{\cdot}273$ (for revolute pin joints) and 1.178 (for spherical socket ball) in the case of unknown loads(or when P is generally larger than 5–8% of $P_{\max}$) will result in a more accurate model than when the conventional model (2) is used.

6. Concluding remarks

In this study, the inclusion of the elastic model between the contacting bodies has resulted in the general formulation of the Coulomb frictional moment in both revolute pin joints and socket-ball joints. The general expression can be written as:

$$M = C_\alpha \frac{F \times R \times \mu}{\sqrt{1+\mu^2}},$$

where the value of C_α can generally be determined for the following three cases:

Case 1: For low contact angles (*e.g.*, $\alpha \leq 20^\circ$), then $C_\alpha \simeq 1$. This corresponds to very light loads (*e.g.*, about or less than 1% of joints allowable loads, Table 2) for which the joints still acts as a rigid body.

Case 2: For partial contact (*e.g.*, $20^\circ < \alpha \leq 90^\circ$) C_α can be calculated by the closed form Equations (17), and (28) for the two cases.

Case 3: For full contact (that $\alpha = 90^\circ$) C_α is equal to $1{\cdot}273(= 4/\pi)$, and $1{\cdot}178(= 3\pi/8)$ for revolute and spherical joints, respectively.

Case 3 is the dominant case for joints operation (more than 90% of the designed load range) that could be used for general estimations when the exact magnitude of load P, or

contact angle α are unknown, but the loads are high enough to cause full contact or near full contact (*e.g.*, $P/P_{\max} > 0{\cdot}08$, Table 2).

In comparison with the conventional friction model (where $C_\alpha = 1$), the new model with a value of C_α obtained according to case 2 or 3 can prevent up to 21% and 15% error in the Coulomb frictional-moment estimation of pin and socket-ball joints, respectively. This higher accuracy is especially important for better control, and dynamic modeling of multi-body systems with several joints in series(with accumulative error. One of such case is the estimation of the frictional moments in the endoscopic flexible stems for locking and motion control of the extenders.

References

1. H. S. Tzou and Y. Rong, Contact dynamics of a spherical joint and a jointed truss-cell system. AAIAA J. 29 (1991) 81–88.
2. R. H. Sturges and S. Laowattana, A flexible, tendon-control device for endoscopy. *Int. J. Robotics Res.* 12 (1993) 121–131.
3. A. Faraz and S. Payandeh, Issues and design concepts in endoscopic extenders. Proc. of 6th IFAC Symp. on Man/Machine Systems. (1995) pp. 109–114.
4. Y. J. Shin and C. H. Kim, An analytical solution for spherical joint mechanism including Coulomb friction. *6th Int. Pacific Conf. Autom. Eng.* (1991) 383–389.
5. L. J. Gutkowski and G. L. Kinzel, A Coulomb friction model for spherical joints. *ASME DE* 45 (1992) 243–250.
6. I. Imam, M. Skrenier and J. P. Sadler, A new solution to Coulomb friction in bearing mechanism: Theory and application. *Trans. ASME* 103 (1981) 764–775.
7. S. A. Lukowski, L. A. Medeksza and P. W. Claar, II, Geometry of contact and Hertzian stress analysis of frictional coupling elements of multidisk stepless transmission with initial point contact. *Trans. ASME, J. Mech. Design* 113 (1991) 416-420.
8. H. Huang and B. Ravani, Contact stress analysis in ball screw mechanism using the tubular medial axis representation of contacting surfaces. *Trans. ASME, J. Mech. Design* 119 (1997) 8–16.
9. J. F. Cuttino and T. A. Dow, Contact between elastic bodies with an elliptic contact interface in torsion. *Trans. ASME, J. Appl. Mech.* 63 (1996) 144–152.
10. J. J. Kalker, F. M. Dekking and E. A. H. Vollebregt, Simulation of rough, elastic contacts. *Trans. ASME, J. Appl. Mech.* 64 (1997) 361–372.
11. M. T. Hanson and I. W. Puja, The elastic field resulting from elliptical Hertzian contact of transversely isotropic bodies: closed-form solutions for normal and shear loading. *Trans. ASME, J. Appl. Mech.* 64 (1997) 457–465.
12. K. L. Johnson, *Contact Mechanics.* Cambridge: Cambridge University Press. (1985) 452 pp.
13. R. G. Budyans, *Advanced Strength and Applied Stress Analysis.* New York: McGraw-Hill (1977) 960 pp.
14. P. F. Byrd and M.D. Friedman, *Handbook of Elliptic Integrals for Engineers and Scientists.* Berlin: Springer-Verlag 358 pp.
15. C. Lipson and R. Juvinall, *Handbook of Stress and Strength.* MacMillan (1963) 447 pp.